

# Estimation of Shape, Volume, and Dipole Moment of Individual Proteins Freely Transiting a Synthetic Nanopore

Jared Houghtaling,<sup>†,‡</sup> Cuifeng Ying,<sup>‡</sup> Olivia M. Eggenberger,<sup>‡</sup> Aziz Fennouri,<sup>‡</sup> Santoshi Nandivada,<sup>§</sup> Mitu Acharjee,<sup>§</sup> Jiali Li,<sup>§</sup> Adam R. Hall,<sup>||</sup> and Michael Mayer<sup>\*,‡</sup>

<sup>†</sup>Department of Biomedical Engineering, University of Michigan, Ann Arbor, Michigan 48109, United States

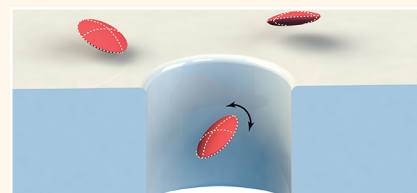
<sup>‡</sup>Adolphe Merkle Institute, University of Fribourg, CH-1700 Fribourg, Switzerland

<sup>§</sup>Department of Physics, University of Arkansas, Fayetteville, Arkansas 72701, United States

<sup>||</sup>Wake Forest University School of Medicine, Winston Salem, North Carolina 27157, United States

## Supporting Information

**ABSTRACT:** This paper demonstrates that high-bandwidth current recordings in combination with low-noise silicon nitride nanopores make it possible to determine the molecular volume, approximate shape, and dipole moment of single native proteins in solution without the need for labeling, tethering, or other chemical modifications of these proteins. The analysis is based on current modulations caused by the translation and rotation of single proteins through a uniform electric field inside of a nanopore. We applied this technique to nine proteins and show that the measured protein parameters agree well with reference values but only if the nanopore walls were coated with a nonstick fluid lipid bilayer. One potential challenge with this approach is that an untethered protein is able to diffuse laterally while transiting a nanopore, which generates increasingly asymmetric disruptions in the electric field as it approaches the nanopore walls. These “off-axis” effects add an additional noise-like element to the electrical recordings, which can be exacerbated by nonspecific interactions with pore walls that are not coated by a fluid lipid bilayer. We performed finite element simulations to quantify the influence of these effects on subsequent analyses. Examining the size, approximate shape, and dipole moment of unperturbed, native proteins in aqueous solution on a single-molecule level in real time while they translocate through a nanopore may enable applications such as identifying or characterizing proteins in a mixture, or monitoring the assembly or disassembly of transient protein complexes based on their shape, volume, or dipole moment.



**KEYWORDS:** nanopores, label-free, single molecule, protein, lipid coating

Recent advances in single-molecule methods, including resistive pulse sensing with nanopores, have made it possible to interrogate the physical characteristics of individual proteins and other biomolecules in aqueous solution.<sup>1–4</sup> Other established biophysical techniques such as atomic force microscopy (AFM) can determine the mechanical properties of proteins in an aqueous sample,<sup>5–7</sup> while optical techniques like fluorescence correlation spectroscopy (FCS)<sup>8–10</sup> and fluorescence resonance energy transfer (FRET)<sup>11–14</sup> reveal spatial and temporal information about single proteins that can provide insight into their structure or interactions with other molecules in solution. For optimal analysis on a single-molecule level, proteins are often subjected to either physical or chemical modifications. These preparation steps can alter intrinsic protein properties and subsequent measurements may not be representative of native proteins in their physiological environments.<sup>5,9,11</sup>

Nanopore-based, resistive pulse sensing is a single-molecule method capable of investigating the physical and structural

properties of individual proteins and protein complexes.<sup>15–29</sup> This technique employs the Coulter counting principle<sup>30</sup> to characterize up to 100 particles per second in electrolyte-rich aqueous solution as they individually transit the zeptoliter confines of a nanopore.<sup>31,32</sup> As shown in Figure 1, each particle disrupts the flow of ions to an extent that depends on its volume, shape, and relative orientation to the electric field, while its dwell time ( $t_d$ ) within the pore corresponds to its net charge and electrophoretic mobility in the applied electric field.<sup>33,34</sup> Resistive pulse-based, nucleic acid sequencing has made notable progress recently by combining biological nanopores with complementary enzymes that ratchet nucleotide strands through the pore one base at a time.<sup>35–46</sup> Protein characterization with nanopores, however, is not as advanced

Received: December 18, 2018

Accepted: April 17, 2019

Published: April 17, 2019

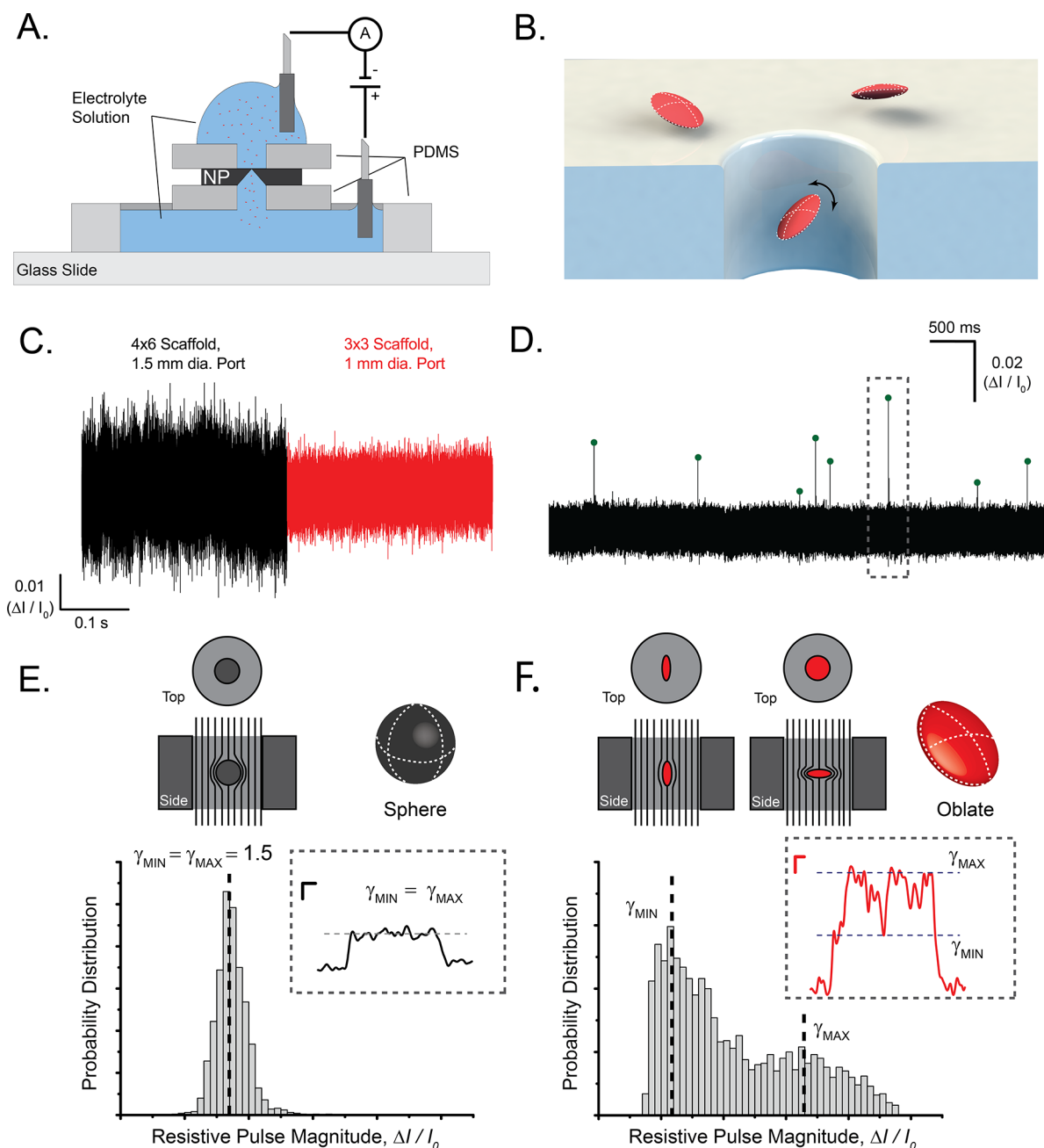


**Figure 1.** Individual, non-spherical proteins passing untethered through a nanopore modulate the conductivity of that pore as a function of their orientation in the pore. These modulations contain information about the length-to-diameter ratios, volumes, and dipole moments of translocating proteins. (A) Schematic cross-section of a setup with a nanopore in a silicon chip and fluid compartments confined by a silicone elastomer (PDMS). (B) Cartoon representation of oblate ellipsoids (red) passing through a nanopore in a free-standing silicon nitride membrane of a nanopore chip. (C) Baseline current measured across the bare (without lipid coating) nanopore substrate at an applied potential difference of  $-100$  mV and digitally filtered with a 50 kHz Gaussian low-pass filter. Both nanopores are approximately 25 nm in diameter. The RMS current noise with the  $3 \times 3$  scaffolds was a factor of 1.8 lower than with the previously used configuration. (D) Example of a current trace with a duration of 10 s, digitally low-pass filtered at 50 kHz, with maximum values of all resistive-pulse events shown as green dots and a long event with a duration greater than  $150 \mu\text{s}$  signified by a dashed gray box. (E, F) Probability distribution of current values within a single resistive pulse as a function of particle length-to-diameter ratio and orientation during its translocation through the nanopore. Inset: original current-vs-time traces of single resistive pulses from the translocation of a streptavidin protein (black) and an IgG protein (red). These traces were digitally low-pass filtered at 10 kHz for clarity. Maximum and minimum blockage values corresponding to electrical shape factors  $\gamma_{\text{max}}$  and  $\gamma_{\text{min}}$  are shown by dashed lines. Scale bars represent  $100 \mu\text{s}$  and  $0.01 (\Delta I / I_0)$ .

as nucleic acid characterization for two key reasons: the size of globular proteins necessitates synthetic nanopores with large diameters that are prone to nonspecific adhesion,<sup>47</sup> and protein characterization targets mobile particles that transit the sensing zone (in the absence of adsorption) at rates approaching or

exceeding the bandwidth of conventional current-recording systems.<sup>48–51</sup>

In response to these challenges, we and others have designed a variety of nanopore systems that slow the transit speeds of proteins while avoiding clogging of the pores. For example,

Wloka *et al.* engineered a nonstick biological nanopore, cytolysin A, with a 5.5 nm diameter sensing vestibule above a 3.8 nm diameter pore and used it to detect the attachment of an individual ubiquitin protein (8.6 kDa) to a protein substrate.<sup>27,52,53</sup> Waduge *et al.* estimated the sizes and intrinsic flexibilities of proteins as they slowly squeezed through synthetic nanopores with diameters only slightly larger than the proteins themselves,<sup>54</sup> while others have investigated protein analytes with a variety of anti-adhesive approaches.<sup>3,55–63</sup> Increasing the viscosity of the recording buffer (e.g., by adding glycerol)<sup>64</sup> also makes it possible to slow the diffusion of proteins, although this approach reduces the conductivity of the recording buffer and thus reduces the amplitude of resistive pulses. Our group introduced a bio-inspired method of coating synthetic nanopores with a fluid lipid bilayer, which prevents or minimizes nonspecific adhesion to the nanopore substrate.<sup>65</sup> This coating can present fluid lipid anchors to slow the diffusion of tethered proteins by taking advantage of the viscosity of the bilayer.<sup>65</sup> We have recently demonstrated the use of lipid-coated nanopores to determine simultaneously the volume, ellipsoidal shape, dipole moment, rotational diffusion coefficient, and charge of proteins in aqueous solution and employed this multi-parametric fingerprint to categorize populations of protein in a binary mixture.<sup>15</sup> For these applications, however, the protein had to be attached to the lipid bilayer by tethering it to a lipid anchor using either chemical cross-linking or a specific lipid-functionalized protein binding complement.

Here, we demonstrate that it is possible to determine the ellipsoidal shape, volume, and dipole moment of single untethered and unmodified proteins in aqueous solution as they translocate through a nanopore, driven by electrophoretic force due to their net charge in the electric field. This approach is different than the method we demonstrated previously because here we allow proteins to diffuse freely in solution and no longer slow their diffusion by tethering them to a lipid anchor in the fluid lipid bilayer. To make this approach possible, we now use nanopore chips with a 3 mm × 3 mm frame, sandwiched between two layers of polydimethylsiloxane (PDMS) with small access ports to the nanopore (Figure 1-A). This experimental design reduced the current noise by 40% at 50 kHz bandwidth and thus increased the signal-to-noise ratio (SNR) at this bandwidth (see Figures 1C and S1) compared with the nanopore setups that we used in previous work.<sup>15,65</sup> By digitally low-pass filtering the data at 50 kHz as opposed to 15 kHz, as we had done previously, we increased the number of analyzable resistive pulses<sup>48,66</sup> as well as the temporal resolution from each translocation event. We show here that the number, duration, and bandwidth of resistive pulses are critical for the accuracy of subsequent analyses on those pulses.

We previously discussed the analysis of data from non-spherical particles rotating in an electric field to calculate protein parameters from individual resistive pulses;<sup>15</sup> the approach is based on fundamental theory developed by Golibersuch and others.<sup>34,60,65,67–72</sup> Briefly, particles rotate and adopt different orientations relative to the electric field during their passage through the pore (Figure 1B). In the case of simple ellipsoidal particles rotating and translocating through a nanopore, an electrical shape factor,  $\gamma$ , relates the particle's orientation,  $\theta$ , within the electric field, and its length-to-diameter ratio,  $m$ , to the current blockade,  $\Delta I/I_0$ . A perfectly spherical particle samples only one  $\gamma$  value (equal to 1.5, Figure 1E) during transit. A non-spherical particle can sample all  $\gamma$

values contained between perfectly cross-wise ( $\gamma_{\max}$ ) and perfectly lengthwise ( $\gamma_{\min}$ ) orientations (Figure 1F) and will do so with a probability for various  $\gamma$  values that can be described by a U-shaped distribution.<sup>34</sup>

To quantify protein length-to-diameter ratio, volume, and dipole moment in this work, we determined the particular probability distribution of  $\gamma$  values for a given protein by using an iterative convolution fitting procedure (see Supplementary Note 1).<sup>15</sup> In this procedure, we fit the entire  $\Delta I/I_0$  distribution from each individual translocation event with a dwell time greater than 150  $\mu\text{s}$  (Figure 1D, gray box). This approach returned an approximate ellipsoidal shape, volume, and dipole moment value for tens to hundreds of individual protein translocation events within a single experiment.

Characterization of freely translocating proteins based on stand-alone analysis of single events one-by-one is uncommon because the majority of work characterizing proteins with nanopores extracts parameters such as volume from populations of resistive pulses rather than from the individual pulses themselves (see Supplementary Note 2). Here, we report all values of volume, length-to-diameter ratio, and dipole moment from individual translocation events as well as the median volume, median length-to-diameter ratio, and the most-probable dipole moment determined from distributions of single-molecule-based individual event analyses (Table S1) and discuss factors that influence the uncertainty of those values. To demonstrate that this characterization methodology can be applied to determine a range of protein characteristics, we chose a set of proteins that vary widely in length-to-diameter ratio ( $m = 0.14$  to 2.5), volume ( $\Lambda = 95$  to 1700 nm<sup>3</sup>), and dipole moment ( $\mu = 484$  to 1846 D). The work presented here demonstrates that, to be feasible, the method combines three important characteristics. First, it estimates multiple physical parameters of proteins translocating freely through a synthetic nanopore by combining low-noise nanopores and high-bandwidth recordings. Second, it proceeds in a more-straightforward manner than its tethered alternative by circumventing the tethering step and thus provides measurements on native, unperturbed proteins. Third, it takes advantage of anti-adhesive nanopore coatings that are critical in providing the free translational and rotational Brownian dynamics necessary to collect these measurements without artifacts.

## RESULTS AND DISCUSSION

**Filtering Attenuates Fluctuations in the Resistive Pulses from Freely Translocating Proteins.** Signal bandwidth is critical for recording accurate amplitudes and durations of resistive pulses; inadequate bandwidth can “clip” the amplitude of the signal or overlook resistive pulses that occur between two sampled points.<sup>75</sup> Moreover, proteins that are not tethered to a lipid bilayer during translocation rotate at a rate that is 2 orders of magnitude faster than tethered proteins.<sup>15,77,80</sup> This difference in rotational diffusion coefficient has important implications when the goal is to resolve time-dependent differences in protein orientation during a single translocation event, as is necessary, for instance, to quantify a bias in orientation that reflects the dipole moment of a protein.

To investigate the extent to which we could resolve different orientations of an untethered protein rotating and translocating freely through a lipid bilayer coated nanopore, we performed random-walk simulations.<sup>15</sup> To do so, we used the

rotational diffusion coefficient of the protein<sup>76</sup> to determine the average rotated angle during each time step around a single rotational axis. We then selected a rotational direction (e.g., clockwise or counterclockwise) based on orientation-dependent biased diffusion in an electric field and converted the resulting array of angles to their corresponding  $\Delta I/I_0$  values.<sup>15</sup> Figure 2 shows ideal representations (i.e., without recording noise) of resistive pulses produced by a simulated random walk for an oblate ellipsoid that represents a 150 kDa protein as it translocates through a nanopore. When the protein rotated with a rotational diffusion coefficient that corresponds to a lipid-anchored state,<sup>15</sup> filtering at 50 kHz retained the large majority of fluctuations as well as their maximum and minimum blockade amplitudes (Figure 2A). This figure panel also shows that to sample both the minimum and the maximum orientations of the particle, dwell times of at least 400  $\mu\text{s}$  duration were required.<sup>15</sup> The reason is that to estimate the ellipsoidal shape,  $m$ , of a protein accurately, the protein must remain sufficiently long in the pore to sample the orientations that correspond to minimum and maximum blockade values because these two values represent the extreme lengthwise and extreme cross-wise orientations of a particle with a given volume and length-to-diameter ratio (see Supplementary eqs 10–15 for how  $(\Delta I/I_0)_{\text{min}}$  and  $(\Delta I/I_0)_{\text{max}}$  influence the quantification of ellipsoidal shape and volume). In contrast, when the protein rotated with a rotational diffusion coefficient that corresponds to bulk solution, a sampling rate of 500 kHz was too slow to completely resolve fluctuations between minimum and maximum orientations, and digital filtering at 50 kHz produced a 41% under-estimate of length-to-diameter ratio as represented by the  $m$  value (Figure 2B). At a rotational diffusion coefficient that was 5-fold slower than bulk, one that describes the protein rotating untethered but within a confined space,<sup>77</sup> sampling at 500 kHz was sufficient to track the protein rotating between minimum and maximum orientations. Low-pass filtering at 50 kHz, however, still produced a 24% underestimate of protein length-to-diameter ratio under these conditions (Figure 2C).

In general, filtering attenuates the current fluctuations that correspond to different orientations of the protein during its translocation through the nanopore. This effect depends on the time resolution of the recording and is pronounced when the protein rotates rapidly, as is the case in Figure 2B. Estimates of length-to-diameter ratio are most influenced by choice of filter cutoff frequency and the rotational diffusion coefficient of the protein (Figure S9A,B). Estimates of volume follow a similar trend to those of length-to-diameter ratio, whereby the estimates are more accurate at higher filter frequencies and slower rotational diffusion coefficients (Figure S9C,D). Estimates of dipole moment, however, appear to be relatively independent of protein rotation rate and filter cutoff frequency (Figure S9E,F) but improve as dwell times increase (Figure S8). These trends highlight the usefulness of anchoring proteins to anti-adhesive coatings to slow both their rotation as well as their speed of transit through the nanopore; they also highlight the importance of attempts to increase recording bandwidth and SNR in future resistive pulse-based experiments for protein characterization. For example, according to Figure 2B, the commercially available Chimera VC-100 amplifier, with a bandwidth of  $\sim 1$  MHz, should be able to time-resolve the rotation of an untethered protein in the confines of a nanopore with significantly higher fidelity than the Axopatch 200B used

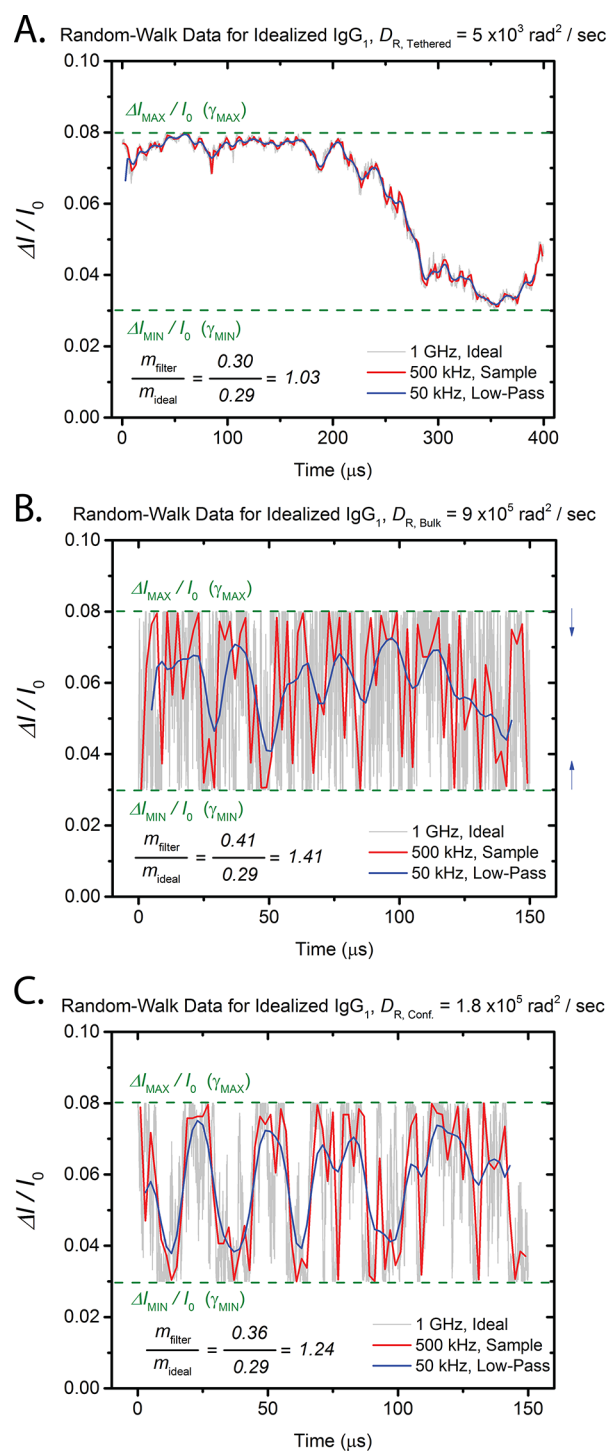


**Figure 2.** Rotational diffusion coefficients affect the ability to resolve protein rotation in time. (A) Simulated resistive-pulse trace generated from a random-walk simulation for a 150 kDa protein with a shape that can be approximated by an oblate ( $m = 0.29$ ,  $\Lambda = 340 \text{ nm}^3$ ,  $\mu = 840 \text{ D}$ ) rotating at a rate of  $5 \times 10^3 \text{ rad}^2 \text{ s}^{-1}$  that corresponds to this protein after tethering it to a lipid bilayer with a lipid anchor as reported by Yusko *et al.*<sup>15</sup> (B) Simulated resistive-pulse trace for the same protein as in panel A rotating with a diffusion coefficient of  $9 \times 10^5 \text{ rad}^2 \text{ s}^{-1}$ , estimated for the particle in bulk solution using the software HydroPRO.<sup>76</sup> Blue arrows show the attenuation effect of low-pass filtering. (C) Simulated resistive-pulse trace for the same protein as in panel A rotating with a rotational diffusion coefficient of  $1.8 \times 10^5 \text{ rad}^2 \text{ s}^{-1}$  that corresponds to an untethered protein inside of the

Figure 2. continued

confinement of a nanopore according to Dix and Verkman.<sup>77</sup> (A–C) Gray lines represent each nanosecond time step of the random-walk simulation. Red lines show the same trace down-sampled at 500 kHz, and the blue lines are the down-sampled trace digitally low-pass filtered at 50 kHz. Note that the blue filtered trace is shifted in time to show visual alignment with other traces (see also [Supplementary Note 2.1](#) and [Figure S3](#)). Green dashed lines show minimum and maximum  $\Delta I/I_0$  values that correspond to electrical shape factors,  $\gamma_{\min}$  and  $\gamma_{\max}$ . Estimated values of protein length-to-diameter ratio,  $m$ , are compared between the filtered data (blue) and the ideal random-walk data (gray). The dwell time of the protein in the pore was set to either (A) 400  $\mu\text{s}$  or (B, C) 150  $\mu\text{s}$ . The electric field within the pore was 1.646  $\text{MV m}^{-1}$ , corresponding to a nanopore with a length of 38 nm and a diameter of 17 nm connected to an adjacent channel with a length of 275 nm and diameter of 100 nm<sup>78</sup> (see [Supplementary Note 1](#)) with an applied potential of 100 mV in 2 M KCl solution with a resistivity of 0.046  $\Omega \text{ m}$ .

here, assuming that the SNR at this bandwidth permits the resolution of various orientations.<sup>66</sup>

With the results from the simulations in [Figure 2](#) in mind, we expected untethered proteins translocating through the confines of a nanopore (analogous to the case illustrated in [Figure 2C](#)) to produce estimates of length-to-diameter ratio,  $m$ , that were less extreme than predicted and thus closer to a sphere ( $m = 1$ ) than to a flattened or elongated ellipsoid of rotation ( $m \ll 1$  or  $m \gg 1$ ). Specifically, data filtered at 50 kHz will not reach the full amplitudes of  $\gamma_{\min}$  and  $\gamma_{\max}$  (blue curve in [Figure 2C](#)) and thus lead to a systematic underestimation of the  $m$  value by approximately 25%.

**Individual Translocations through Lipid Bilayer-Coated Nanopores and Information about Protein Ellipsoidal Shape, Volume, and Dipole Moment.** [Figure 3 A,C](#) shows individual data of experimental length-to-diameter ratio and volume determinations that resulted from individual translocation events of a single protein moving through the nanopore. To allow for sufficient time such that proteins could sample all electrical shape factors, we restricted the analysis to resistive pulses with a duration of at least 150  $\mu\text{s}$ . As shown in [Figure 3B,D](#), determined values for length-to-diameter ratio and volume were in reasonable agreement with reference values: median estimates for the length-to-diameter ratio deviated on average by 35% from reference values across all proteins, and median volume estimates were within 40% of reference values. [Figure 3](#) also shows that estimates of protein length-to-diameter ratio, volume, and dipole moment from individual translocation events varied considerably for each protein. We attribute this variability to the intrinsic uncertainty of single-molecule analyses,<sup>73,74</sup> to noise in the signal recording,<sup>75</sup> to the limited recording bandwidth,<sup>75</sup> to the fundamental limitation of approximating a complex three-dimensional protein shape with a simple ellipsoid (see [Supplementary Note 7](#) and [Figure S10](#) for details on the accuracy of this approximation) and to off-axis effects, as discussed below.<sup>33</sup> We note that the approach of analyzing single translocation events in a stand-alone fashion as shown in [Figure 3A,C,E](#) is particularly demanding and thus the median length-to-diameter ratio and volume estimates from these analyses were less accurate than estimates from population-based analyses, similar to findings from previous work.<sup>15</sup> For instance, population-based analyses performed on the same

data revealed protein length-to-diameter ratios that were within 20% of reference values for all oblate-shaped proteins, and volume estimates that were strongly correlated with reference values for all nine proteins (slope of 0.989 and Pearson's  $r$  of 0.99; see [Supplementary Note 2](#) and [Figure S2](#)). The reason why we emphasized stand-alone event-by-event analysis in the work presented here is that single-event analysis is required to achieve the long-term goal of analyzing mixtures of proteins.

Proteins with a permanent dipole moment do not rotate randomly while passing through the electric field within a nanopore; rather, they experience a Brownian rotation that is biased by torque acting on their dipole from the electric field.<sup>79</sup> The convolution-based model used to fit the data in this work accounted for this bias (see [Supplementary Note 1](#)) and ultimately determined the extent of bias each protein had for its minimum ( $\gamma_{\min}$ ) and maximum ( $\gamma_{\max}$ ) electrical shape factors; *i.e.*, did the protein sample both maxima with equal probability, or did it sample one orientation and hence electrical shape factor more often than the other? [Figure 3F](#) shows the most-probable dipole moment values ( $\mu$ ) determined through log-normal fitting of the distribution of measured dipoles for each protein.<sup>15</sup> These dipole estimates were in good agreement with reference values; most-probable dipole moment estimates for each protein deviated on average by less than 20% from their reference values. Event-to-event variability in dipole moment was large ([Figure 3E](#)), consistent with the data spread in length-to-diameter ratio and volume estimates; the estimates of dipole moment for individual BSA events, for example, had a median absolute deviation of 73%. While this level of uncertainty is relatively high, we note that this is the only technique available to estimate the dipole moment of individual unmodified proteins in solution. In our previous work,<sup>15</sup> tethering removed one positive charge from each protein when cross-linking them to a lipid anchor in the bilayer by means of a bifunctional *N*-hydroxysuccinimide (NHS) linker. Removing a charge of a randomly located amine on the surface of the protein inherently distorted that protein's permanent dipole moment and is thus not desirable.<sup>15</sup> Furthermore, the technique presented here generates dipole estimates within a few hundred microseconds as the protein passes through the nanopore and is compatible with small sample volumes ranging from nano- to microliters as well as low protein concentrations ranging from nano- to micromolar. These characteristics are attractive because dipole moments are becoming increasingly important for the rheological properties of concentrated antibody formulations used for subcutaneous administration.<sup>81</sup> Rapid quantification of dipole moments in aqueous solution also provides additional discriminatory power in heterogeneous protein mixtures as dipole moments are distributed broadly between different proteins and show little to no correlation with the volume or length-to-diameter ratio of proteins.<sup>15</sup>

In previous work on lipid-anchored proteins, we restricted the analyses to individual resistive pulses longer than 400  $\mu\text{s}$  because we could be confident that most tethered proteins would sample all possible orientation-dependent electrical shape factors ( $\gamma$ ) within this time frame ([Figure 2A](#)).<sup>15</sup> Proteins that rotate freely in bulk solution, however, do so at a rate 2 orders of magnitude faster than tethered proteins inside of a nanopore,<sup>15,80</sup> and thus, freely translocating proteins sample all possible  $\gamma$  values on much shorter time scales than tethered proteins. When selecting a threshold for sufficiently

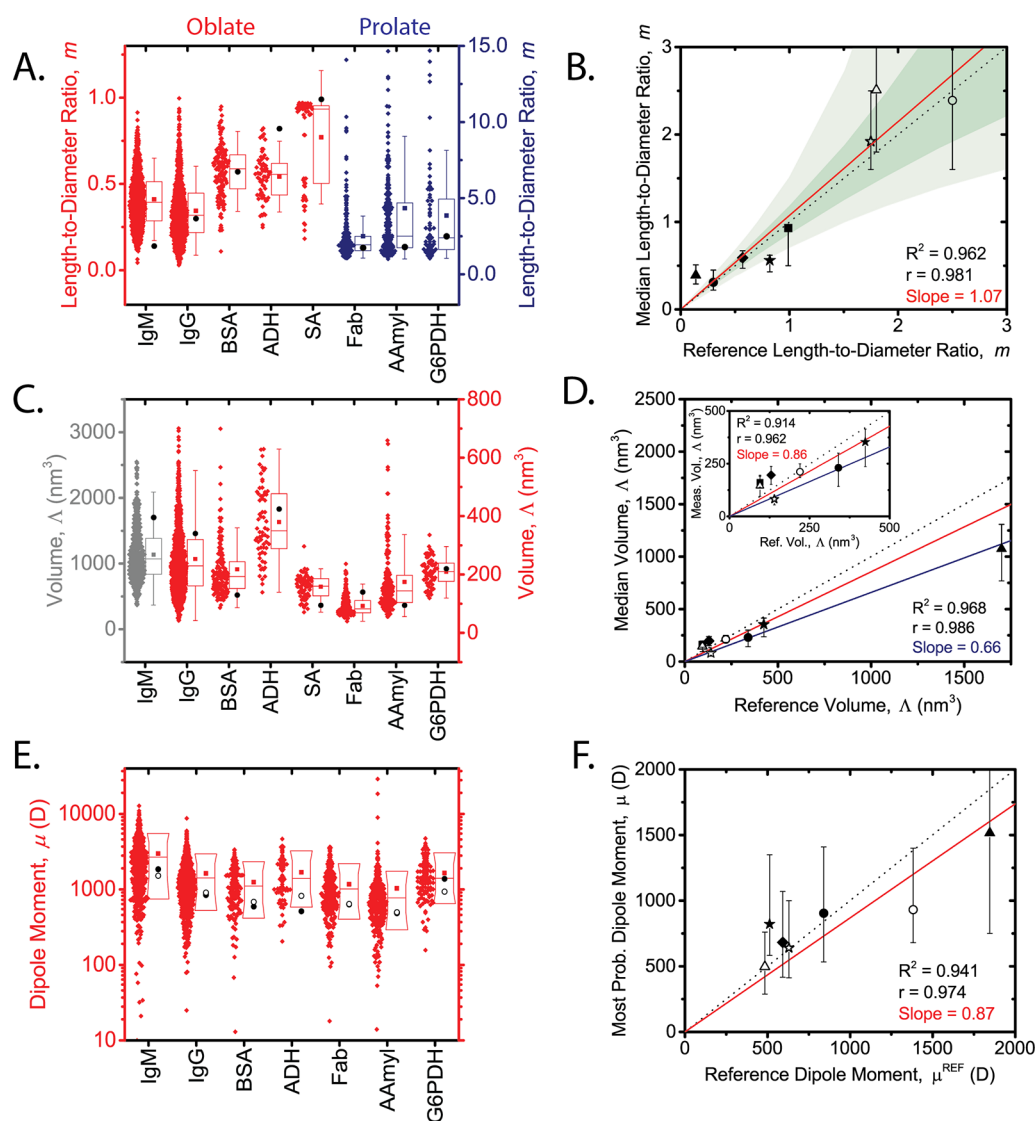


**Figure 3.** Individual-event analyses of experiments performed on lipid bilayer-coated nanopores produce good estimates of protein length-to-diameter ratio, volume, and dipole moment. (A) Length-to-diameter ratios determined from individual resistive pulses from the translocation of various oblate-shaped proteins (red) and various prolate-shaped proteins (blue). (B) Comparison of the median values of measured length-to-diameter ratios,  $m$ , with reference values for each protein. The red line is the linear fit for all proteins in the study, the black dotted line shows the ideal 1:1 agreement, and the dark and light green regions represent estimates of length-to-diameter ratio in the presence of  $\pm 10\%$  and  $\pm 25\%$  deviations in minimum and maximum blockade values, respectively. Error bars show first and third quartiles. (C) Volumes of all proteins, with IgM in gray corresponding to the left y-axis in gray and other proteins in red corresponding to the right y-axis in red. (D) Comparison of the median values of the volumes for 8 proteins determined from single event analyses with reference values for these proteins. Inset shows values for proteins with volumes smaller than  $500 \text{ nm}^3$ . The red line represents a linear fit for only the proteins with volumes smaller than  $500 \text{ nm}^3$ , and the blue line represents a linear fit through data for all proteins. Error bars show the first and third quartile. (E) Dipole moment estimates for individual events of all non-spherical proteins. Data are plotted on a log scale to represent their underlying log-normal distribution, as discussed by Yusko *et al.*<sup>15</sup> Boxes span the 10th to 90th percentile of the data. (A, C, E) Parameter estimates from individual long events are shown as red diamonds, red squares represent mean values, horizontal lines represent median and quartile values, whiskers represent the standard deviation of the values, solid black circles denote reference values, and black open circles denote most-probable values determined through log-normal fitting.<sup>15</sup> (F) Comparison of estimated dipole moments with reference values for all seven non-spherical proteins investigated. The black dotted line represents the ideal 1:1 agreement, and the red solid line is the linear fit. Error bars range from the 10th to the 50th percentile. (B, D, F) Proteins are plotted as follows: antibiotin Fab (open stars,  $N = 271$ ),  $\alpha$ -amylase (open triangles,  $N = 222$ ),  $G_6$ PDH (open circles,  $N = 72$ ), IgM (triangles,  $N = 743$ ), antibiotin IgG<sub>1</sub> (circles,  $N = 955$ ), BSA (diamonds,  $N = 144$ ), ADH (stars,  $N = 66$ ), and streptavidin (squares,  $N = 67$ ). See Table S1 for quantitative values.

long events, we struck a balance between accuracy and sample size (see Supplementary Note 2.2 and Figure S8). In other words, we needed to gather current-versus-time data with sufficient duration to produce accurate estimates of protein parameters, but we also needed to collect as many events as possible for analysis within a standard experimental time frame.

Based on theoretical predictions using a model that treats translocations of charged proteins as a biased first-passage-time problem,<sup>82</sup> we estimated that the most-probable dwell times for the proteins in this study were all shorter than  $10 \mu\text{s}$  (see Supplementary Note 3). Hence, only a small percentage ( $<1\%$ ) of the total number of translocation events that we resolved

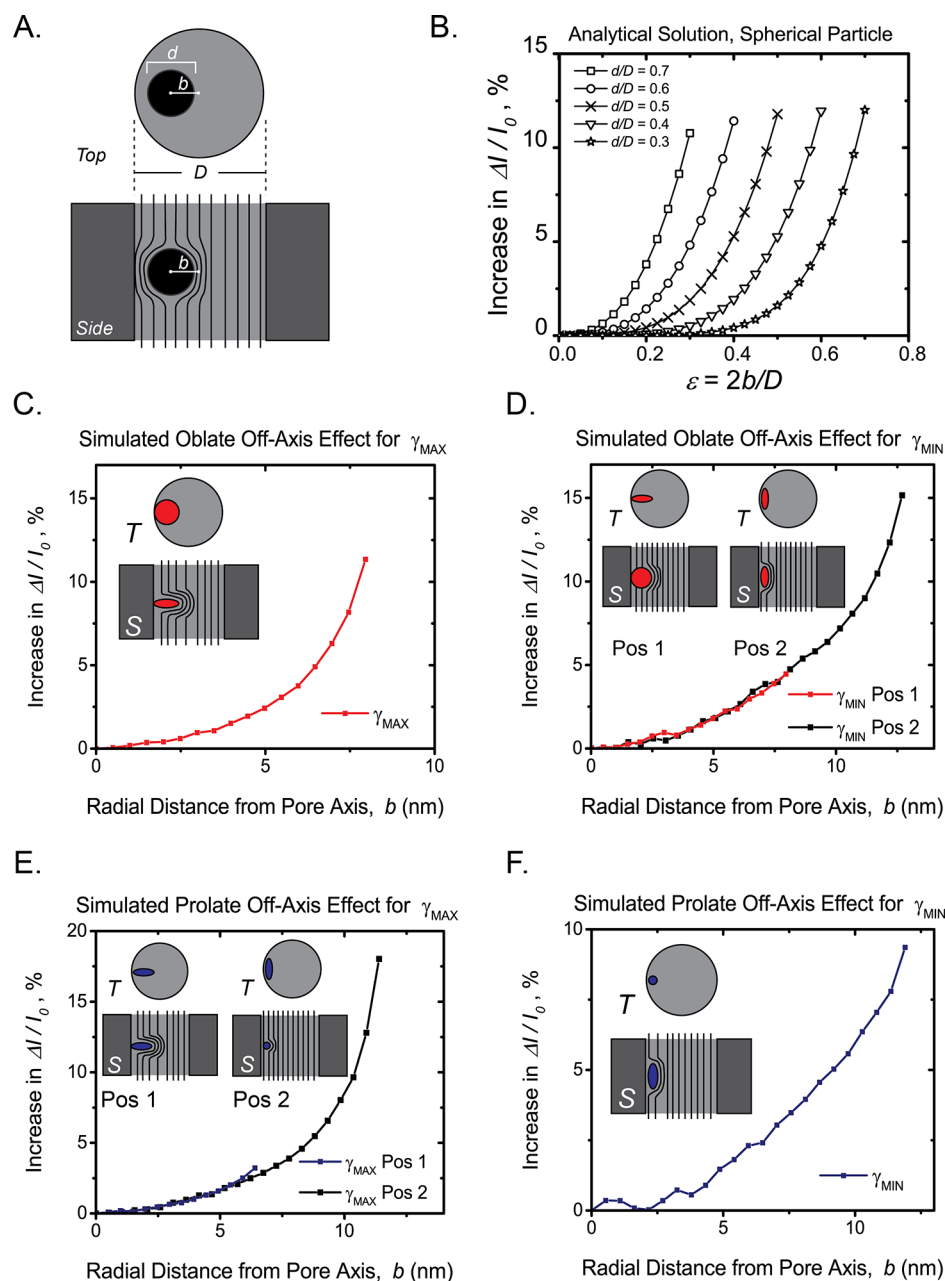


**Figure 4.** Off-axis effects during the translocation of non-spherical particles through a nanopore are orientation-dependent and can produce 18% deviations in resistive pulse magnitude. (A) Schematic of a spherical particle (black) passing through a pore (gray). The diameter of the particle is denoted as  $d$ , the diameter of the pore is labeled  $D$ , and the radial distance from the center of the pore is labeled  $b$ . (B) Analytical solutions according to Qin *et al.*<sup>33</sup> showing the magnitude of off-axis effects on the magnitude of the resistive pulse labeled as an increase in  $\Delta I / I_0$  in the scenario in which a perfectly spherical particle transits a cylindrical nanopore. The  $x$ -axis represents  $\epsilon$ , which relates the off-axis distance to the pore diameter. (C–F) Plots generated using finite element simulations (COMSOL) showing the increase of the magnitude of resistive pulses for both oblate (panels C and D) and prolate (panels E and F) proteins at orientations that produce a maximum blockade (panels C and E) and a minimum blockade (panels D and F). For the oblate scenario, the simulation was conducted using a particle with a size and shape similar to an IgG<sub>1</sub> antibody ( $m = 0.2$ ,  $\Lambda = 275.6 \text{ nm}^3$ ) passing through a pore with a 30 nm diameter and a 30 nm length. For the prolate scenario, the simulation was conducted using a particle with a size and shape similar to G6PDH ( $m = 3.0$ ,  $\Lambda = 268.4 \text{ nm}^3$ ) passing through a pore with a 30 nm diameter and a 30 nm length. For non-spherical particles, we defined  $b$  as the distance from the central axis of the pore to the center of mass of the particle.

had dwell times longer than  $150 \mu\text{s}$ .<sup>15,48,65</sup> Nonetheless, we found that a threshold of  $150 \mu\text{s}$  was the optimal choice for our recording setup combined with a digital Gaussian low-pass filter with a cutoff frequency of 50 kHz, rather than the 15 kHz filter that we used in previous work.<sup>15</sup> This elevated cutoff frequency made it possible to time-resolve a larger fraction of high-frequency protein movement and to reduce the rise time

of the digital filter and thus increase the fraction of each resistive pulse that could be analyzed (Figure 2C). Unexpectedly, the values that we determined for the length-to-diameter ratio of eight proteins after filtering the data with this low-pass filter were not systematically attenuated as the simulations in Figure 2C predicted; rather, they varied evenly over all proteins (slope of 1.07). Figure 4 shows that this

better-than-expected agreement between simulation and experiment arose, at least in part, from off-axis effects that influenced resistive pulse amplitudes and acted to shift determined ellipsoidal shapes toward more extreme values.

To determine if the analysis approach presented here could be applied in the context of commonly used antiadhesive coatings other than lipid bilayers, we also performed experiments with Tween-20 coated nanopores (see [Supplementary Note 4](#)) following the protocol of Li *et al.*<sup>83</sup> This coating is attractive because it is more straightforward to prepare than lipid bilayer coatings of high quality. We found that while volume estimates from a Tween-20 coated pore agreed with reference values, the estimates for length-to-diameter ratio were skewed toward an  $m$  value of 0.5, and estimates for dipole moment showed a weak correlation with reference values (see [Figure S5D](#)). Additionally, the event frequencies and protein dwell times that we observed with Tween-20 coated nanopores did not correspond to freely translocating proteins. For example, we recorded an average event frequency of 1.7 Hz for alcohol dehydrogenase (ADH) at a protein concentration of 80 nM in a Tween-20 coated pore. A theoretical analysis following the approach by Plesa *et al.*<sup>48</sup> predicts a detection frequency of only 0.02 Hz at this protein concentration. The reason why we experimentally observed almost 100-fold more frequent translocations than theoretically expected at the bandwidth of our experiments is that the protein's residence times in the Tween-20 coated pore were significantly longer than predicted. We attribute this observation to nonspecific interactions with the pore walls,<sup>51</sup> possibly in combination with electroosmotic flow (EOF) mediated by residual surface charge in nanopores coated with Tween-20.<sup>84</sup> In contrast, when we used nanopores that were coated with a lipid bilayer, the theoretical predictions of event frequencies were in excellent agreement with experimentally observed event frequencies. For instance, at a concentration of 10  $\mu$ M ADH, we observed an event frequency of 1.2 Hz using a lipid bilayer coated pore; the theoretical prediction was 1–5 Hz at this protein concentration. If significant nonspecific interactions of the protein with the pore wall would have been present, then our experimentally observed detection frequency would again have been significantly higher than the theoretical prediction, and we would have expected to observe differences in estimates of protein parameters between the shortest and longest translocation events for a given protein (see [Supplementary Note 6](#) and [Figures S6 and S7](#)).

While the Tween-20 surface coating could not completely circumvent EOF and adhesive interactions with the pore wall, it did prevent clogging of the nanopore and enabled the accurate estimation of protein volumes (see [Figure S5C](#)) as reported previously.<sup>50,83</sup> When we used pores in silicon nitride without any surface coating, we encountered clogging during translocation experiments of ferritin and IgM proteins at typically employed concentrations between 0.1 and 1  $\mu$ M, which terminated the experiments. Adhesive interactions with the Tween-20-coated nanopore walls, however, led to inaccurate quantification of protein length-to-diameter ratio and dipole moment (see [Supplementary Note 4](#) and [Figure S5](#)). Therefore, the results with Tween-20 highlight the benefits of lipid bilayer coatings in providing nonstick synthetic nanopores with almost completely suppressed EOF.<sup>85,86</sup>

**Off-Axis Effects and Distortion of Resistive Pulse Magnitudes.** The analysis that we used to determine the length-to-diameter ratio and, in particular, the dipole moment

of proteins requires that the protein is able to rotate unperturbed within the nanopore. It follows that the diameter of the nanopore must be larger than the largest dimension of the protein, which inherently means that the protein has space to diffuse laterally within the pore during its translocation.<sup>15</sup> Proteins that translocate untethered, therefore, may be electrically sampled at the center of the pore, at the pore wall, or anywhere in between, limited only by steric hindrance and random diffusion.<sup>33,50</sup> When a particle transits a nanopore not through the very center but at some radial distance  $b$  from the central pore axis, it distorts the electric field within the pore asymmetrically.<sup>33</sup> This asymmetrical disruption produces a larger-than-expected resistive pulse whose magnitude depends on the particle's off-axis distance ( $b$ ) and on the ratio of particle diameter to pore diameter ([Figure 4A,B](#)). This phenomenon, known as an off-axis effect, has been studied sporadically in the context of Coulter counters since the 1970s;<sup>87,88</sup> it has attracted renewed consideration as research groups are beginning to perform finite element simulations on nanopore systems and as the analysis of resistive pulses from single macromolecules is becoming increasingly sophisticated and information-rich.<sup>33,89–92</sup>

To provide insight into the extent to which off-axis effects influence the parameter estimates of freely translocating non-spherical proteins, as opposed to spherical proteins,<sup>33</sup> we performed finite element simulations of ellipsoidal particles passing through a cylindrical nanopore at various distances from the central axis (see [Supplementary Note 5](#)). [Figure 4C–F](#) shows the results of these simulations, carried out for relatively extreme oblate-shaped and prolate-shaped particles in their orientations of minimum and maximum electrical shape factor,  $\gamma$ , relative to the electric field. We found that for the range of nanopore and protein sizes that are typically used for protein characterization, and in the most extreme off-axis scenario (prolate-shaped particle,  $\gamma_{\max}$ ,  $b_{\max}$ ), these effects can distort the resistive pulse magnitudes of non-spherical particles by up to 18%. An untethered protein may therefore sample its maximum blockade orientation near the pore wall, and its minimum blockade orientation near the central pore axis, leading to a larger difference between maximum and minimum blockade values and thus to a more extreme estimate for protein length-to-diameter ratio than if the protein transited only through the central pore axis. With regard to the resulting error in length-to-diameter ratio estimates, this distortion falls within the green shaded regions in [Figure 3B](#) and likely contributes to the spread of the data in [Figure 3A](#). We see that off-axis translocation has a stronger influence on parameter estimates for prolate-shaped particles than for oblate-shaped particles; this result agrees with the uncertainty in the length-to-diameter ratio estimates for prolate-shaped proteins (see also [Supplementary Note 2](#)). We suggest that the off-axis effect on resistive pulse signals can be viewed as another contributor to the overall noise in the system, with a frequency component related to the lateral diffusion coefficient of the protein within the pore. Hence, off-axis effects contributed to the variability in calculated parameter values, especially for analyses of individual events, but they did not preclude the determination of protein parameters, as evidenced by the agreement of parameter estimates with reference values in [Figure 3](#). Furthermore, and fortuitously for this work, off-axis effects, which led to estimates of particle length-to-diameter ratio that were more extreme than those from experiments without off-axis effects, offset the effects of filtering, which led to estimates

of particle length-to-diameter ratio that were less extreme than those revealed from experiments with adequate bandwidth (e.g., greater than 500 kHz). It appears, therefore, that these two opposing effects canceled each other to some extent and led to the good agreement between experimental and reference length-to-diameter ratios reported in Figure 3. Based on these arguments, off-axis effects will become more dominant in scenarios with higher bandwidths and lower noise levels than the recording setup used here and will need to be considered in future efforts to improve analysis methods of particles translocating freely and untethered through nanopores.

## CONCLUSIONS

This work estimates three distinct protein parameters from the resistive pulses generated by single native and untethered proteins passing through a lipid-coated synthetic nanopore. Among these parameters is dipole moment, which can be quantified on a single-molecule level for unmodified proteins in solution. No other technique has this capability, and given the increasing importance of dipole moments for formulations of monoclonal antibodies,<sup>81</sup> this capability may accelerate the development of formulations for subcutaneous administration of therapeutic antibodies; the fastest growing class of therapeutics.<sup>93</sup> In addition, dipole moment is an excellent protein descriptor that is orthogonal to protein volume and shape,<sup>15</sup> such that simultaneous quantification of these three parameters in sub-millisecond time frames of unmodified proteins in solution may enable plug-and-play benchtop protein analysis systems that characterize and count single proteins. The approach introduced here can likely be optimized: ongoing improvements in SNR will reduce the spread in parameter estimates,<sup>94–97</sup> and further increases in recording bandwidth through improved CMOS current amplifiers<sup>66</sup> will increase event capture rates, resolve larger fractions of  $t_d$  distributions, and monitor information about protein rotation and shape at smaller time steps. Each of these improvements will further reduce the uncertainty of nanopore-based characterization of single proteins.

The work presented here reaffirms the critical importance of anti-adhesive coatings in nanopore-based analyses that rely on translational and rotational dynamics of proteins in an electric field<sup>15,61,65,83,98,99</sup> and highlights the need for developing future systems that confine proteins to a single translocation axis rather than allowing them to diffuse laterally within the pore. However, perhaps the most promising aspect of the nanopore-based analysis technique presented here is that it has the potential to probe native proteins and protein complexes that are transient in nature, including amyloids and amyloid oligomers, without the need for modifications.<sup>3,4</sup> Interest in characterizing this class of heterogeneous protein analytes with nanopores is growing,<sup>50,61,100,101</sup> and the single-particle analysis approach that we present here adds additional protein descriptors such as shape and dipole moment to particle volume and charge. Together, these parameters may be useful for correlating the physical characteristics such as the size and shape of various amyloid species with their toxicity<sup>102</sup> as well as for defining and detecting biomarkers that reveal disease progression or the efficacy of therapeutics at early stages of amyloid-induced neurodegenerative diseases.<sup>8,103</sup>

## MATERIALS AND METHODS

**Materials.** We purchased all phospholipids, namely 1-palmitoyl-2-oleoyl-*sn*-glycero-3-phosphocholine (POPC) and 1,2-dipalmitoyl-*sn*-

glycero-3-phosphoethanolamine-*N*-(lissamine rhodamine B sulphonyl) (Rh-PE), from Avanti Polar Lipids. Monoclonal anti-biotin IgG1 (B7653), glucose-6-phosphate dehydrogenase (G5885), IgM from human serum (I8260), bovine serum albumin (A7638),  $\alpha$ -amylase (A4551), streptavidin from *Streptomyces avidinii* (85878), alcohol dehydrogenase from *Saccharomyces cerevisiae* (A7011), and ferritin from human liver (F6754) were purchased from Sigma-Aldrich. Polyclonal anti-biotin IgG-Fab fragments (800-101-098) were purchased from Rockland Immunochemicals. We investigated the purity of each sample using size-exclusion high-performance liquid chromatography with an Agilent SEC3 column (300 mm, 300 nm pore size, 4.6 mm internal diameter) using 1× PBS plus 1 mM EDTA as the running buffer at 0.3 mL min<sup>-1</sup> and include the results of this investigation in Supplementary Note 8, Figure S11, and Table S4.

**Setup and Experimental Details.** Nanopores were fabricated in a silicon nitride membrane, 275 nm thick, supported by a silicon chip, 3 mm × 3 mm square, using an ion-beam sculpting technique (see Supplementary Note 1 for details on pore geometry).<sup>78</sup> Experiments using Tween-20 coated pores (see Supplementary Note 4) were performed both on these ion-beam-sculpted nanopores as well as on nanopores generated using a helium ion microscope drilling technique.<sup>104</sup> Before each experiment, we cleaned nanopores in a freshly mixed Piranha solution containing 3:1 (v/v) concentrated sulfuric acid and aqueous hydrogen peroxide solution at a temperature of 60–70 °C for at least 30 min, rinsed the chips copiously with deionized water, and dried them with nitrogen gas. We then mounted the chips between two pieces of cured PDMS containing ports with a 1 mm diameter for access the nanopore to separate *cis* and *trans* electrolyte reservoirs (Figure 1A). The active lead of the headstage of the amplifier was connected to the *cis* compartment, while the ground lead of the headstage was connected to the *trans* compartment. To apply the lipid coatings, we formed supported lipid bilayers with 0.8 mol % of fluorescently labeled lipid, Rh-PE, in 99.2 mol % POPC through fusion of small unilamellar vesicles (SUVs), which were prepared in a buffer containing 150 mM KCl and 10 mM HEPES at pH 7.4 for 20 min before being thoroughly rinsed with deionized water and then replacing the solution in both compartments with a recording buffer (2 M KCl), as described previously.<sup>65</sup> To perform the experiments, we placed the experimental setup with the nanopore chip in a Faraday cage, immersing Ag/AgCl pellet electrodes (Warner Instruments) into their respective electrolyte compartments. We applied a constant potential of  $\pm(100$  to 150) mV across the nanopore and then measured the current (500 kHz sampling rate via NI PCI 6281 or USB-6361, 100 kHz analog low-pass filter,  $f_c = 50$  kHz digital Gaussian low-pass FIR filter of length  $L = 2N + 1$  with delay of  $N/SR$  seconds) using an AxoPatch 200B (Molecular Devices) patch-clamp amplifier in voltage-clamp mode ( $\beta = 1$ ) in combination with LabVIEW (National Instruments) software. We defined a resistive pulse by a reduction of the baseline current that exceeded a threshold of 5× the standard deviation of the noise and marked the beginning and end of that resistive pulse where the current started and returned to within 1× standard deviation of the baseline.<sup>105</sup> We defined the translocation time of each event as the full-width at half-maximum value of that resistive pulse. All peak-finding and analysis procedures were performed using MATLAB (MathWorks) software. We describe these fitting procedures, namely the convolution model, in detail in Supplementary Note 1.<sup>15</sup>

**Finite Element Simulations with COMSOL.** We performed finite element simulations, shown graphically in Figure 4, using COMSOL Multiphysics 5.3a. We outline the parameters used for these simulations in Supplementary Note 5.

## ASSOCIATED CONTENT

### Supporting Information

The Supporting Information is available free of charge on the ACS Publications website at DOI: 10.1021/acsnano.8b09555.

Detailed descriptions of the convolution model, population-based analyses of resistive pulses, threshold selections for different analysis methods, control experi-

ments with Tween-20 nanopore coatings, COMSOL simulations for estimating off-axis effects, comparisons of resistive pulses with different dwell times, limitations of the ellipsoidal approximation, and investigation of protein purity (PDF)

## AUTHOR INFORMATION

### Corresponding Author

\*E-mail: michael.mayer@unifr.ch.

### ORCID

Jared Houghtaling: 0000-0003-1557-9716

Cuifeng Ying: 0000-0002-7279-1388

Aziz Fennouri: 0000-0003-0922-2745

Jiali Li: 0000-0002-8198-1132

Adam R. Hall: 0000-0003-2053-6075

### Notes

The authors declare no competing financial interest.

## ACKNOWLEDGMENTS

This work was financially supported through the Adolphe Merkle Foundation, Oxford Nanopore Technologies (M.M., grant no. 350509-N016133), the Swiss National Science Foundation (M.M., grant no. 200021-169304), and a Graduate Research Fellowship from the U.S. National Science Foundation (J.H.).

## REFERENCES

- (1) Han, A.; Schürmann, G.; Mondin, G.; Bitterli, R. A.; Hegelbach, N. G.; de Rooij, N. F.; Staufer, U. Sensing Protein Molecules Using Nanofabricated Pores. *Appl. Phys. Lett.* **2006**, *88*, 093901.
- (2) Li, J.; Gershow, M.; Stein, D.; Brandin, E.; Golovchenko, J. A. DNA Molecules and Configurations in a Solid-State Nanopore Microscope. *Nat. Mater.* **2003**, *2*, 611.
- (3) Yusko, E. C.; Prangkio, P.; Sept, D.; Rollings, R. C.; Li, J.; Mayer, M. Single-Particle Characterization of  $\alpha\beta$  Oligomers in Solution. *ACS Nano* **2012**, *6*, 5909–5919.
- (4) Houghtaling, J.; List, J.; Mayer, M. Nanopore-Based, Rapid Characterization of Individual Amyloid Particles in Solution: Concepts, Challenges, and Prospects. *Small* **2018**, *14*, 1802412.
- (5) Moore, S. W.; Roca-Cusachs, P.; Sheetz, M. P. Stretchy Proteins on Stretchy Substrates: The Important Elements of Integrin-Mediated Rigidity Sensing. *Dev. Cell* **2010**, *19*, 194–206.
- (6) Afrin, R.; Alam, M. T.; Ikai, A. Pretransition and Progressive Softening of Bovine Carbonic Anhydrase II as Probed by Single Molecule Atomic Force Microscopy. *Protein Sci.* **2005**, *14*, 1447–1457.
- (7) Nirmalraj, P.; Thompson, D.; Molina-Ontoria, A.; Sousa, M.; Martín, N.; Gotsmann, B.; Riel, H. Nanoelectrical Analysis of Single Molecules and Atomic-Scale Materials at the Solid/Liquid Interface. *Nat. Mater.* **2014**, *13*, 947–953.
- (8) Kaye, R.; Head, E.; Thompson, J. L.; McIntire, T. M.; Milton, S. C.; Cotman, C. W.; Glabe, C. G. Common Structure of Soluble Amyloid Oligomers Implies Common Mechanism of Pathogenesis. *Science* **2003**, *300*, 486–489.
- (9) Eggeling, C.; Ringemann, C.; Medda, R.; Schwarzmann, G.; Sandhoff, K.; Polyakova, S.; Belov, V. N.; Hein, B.; von Middendorff, C.; Schoenle, A.; Hell, S. W. Direct Observation of the Nanoscale Dynamics of Membrane Lipids in a Living Cell. *Nature* **2009**, *457*, 1159–1121.
- (10) Yang, H.; Luo, G. B.; Karnchanaphanurach, P.; Louie, T. M.; Rech, I.; Cova, S.; Xun, L. Y.; Xie, X. S. Protein Conformational Dynamics Probed by Single-Molecule Electron Transfer. *Science* **2003**, *302*, 262–266.
- (11) Schuler, B.; Eaton, W. A. Protein Folding Studied by Single-Molecule FRET. *Curr. Opin. Struct. Biol.* **2008**, *18*, 16–26.
- (12) Deniz, A. A.; Laurence, T. A.; Beligere, G. S.; Dahan, M.; Martin, A. B.; Chemla, D. S.; Dawson, P. E.; Schultz, P. G.; Weiss, S. Single-Molecule Protein Folding: Diffusion Fluorescence Resonance Energy Transfer Studies of the Denaturation of Chymotrypsin Inhibitor 2. *Proc. Natl. Acad. Sci. U. S. A.* **2000**, *97*, 5179–5184.
- (13) Merchant, K. A.; Best, R. B.; Louis, J. M.; Gopich, I. V.; Eaton, W. A. Characterizing the Unfolded States of Proteins Using Single-Molecule FRET Spectroscopy and Molecular Simulations. *Proc. Natl. Acad. Sci. U. S. A.* **2007**, *104*, 1528–1533.
- (14) Jares-Erijman, E. A.; Jovin, T. M. FRET Imaging. *Nat. Biotechnol.* **2003**, *21*, 1387–1395.
- (15) Yusko, E. C.; Bruhn, B. R.; Eggenberger, O. M.; Houghtaling, J.; Rollings, R. C.; Walsh, N. C.; Nandivada, S.; Pindrus, M.; Hall, A. R.; Sept, D.; Li, J.; Kalonia, D. S.; Mayer, M. Real-Time Shape Approximation and Fingerprinting of Single Proteins Using a Nanopore. *Nat. Nanotechnol.* **2017**, *12*, 360–367.
- (16) Ivankin, A.; Carson, S.; Kinney, S. R.; Wanunu, M. Fast, Label-Free Force Spectroscopy of Histone-DNA Interactions in Individual Nucleosomes Using Nanopores. *J. Am. Chem. Soc.* **2013**, *135*, 15350–15352.
- (17) Ananth, A.; Genua, M.; Aissaoui, N.; Díaz, L.; Eisele, N. B.; Frey, S.; Dekker, C.; Richter, R. P.; Görlich, D. Reversible Immobilization of Proteins in Sensors and Solid-State Nanopores. *Small* **2018**, *14*, 1703357.
- (18) Soni, G. V.; Dekker, C. Detection of Nucleosomal Substructures Using Solid-State Nanopores. *Nano Lett.* **2012**, *12*, 3180–3186.
- (19) Rivas, F.; Zahid, O. K.; Reesink, H. L.; Peal, B. T.; Nixon, A. J.; DeAngelis, P. L.; Skardal, A.; Rahbar, E.; Hall, A. R. Label-Free Analysis of Physiological Hyaluronan Size Distribution with a Solid-State Nanopore Sensor. *Nat. Commun.* **2018**, *9*, 1037.
- (20) Kasianowicz, J. J.; Bezrukov, S. M. Protonation Dynamics of the Alpha-Toxin Ion Channel from Spectral Analysis of PH-Dependent Current Fluctuations. *Biophys. J.* **1995**, *69*, 94–105.
- (21) Kasianowicz, J. J.; Balijepalli, A. K.; Etedgui, J.; Forstater, J. H.; Wang, H.; Zhang, H.; Robertson, J. W. Analytical Applications for Pore-Forming Proteins. *Biochim. Biophys. Acta, Biomembr.* **2016**, *1858*, 593–606.
- (22) Bezrukov, S. M.; Kasianowicz, J. J. Current Noise Reveals Protonation Kinetics and Number of Ionizable Sites in an Open Protein Ion Channel. *Phys. Rev. Lett.* **1993**, *70*, 2352–2355.
- (23) Oukhaled, A.; Cressiot, B.; Bacri, L.; Pastoriza-Gallego, M.; Betton, J.-M.; Bourhis, E.; Jede, R.; Gierak, J.; Auvray, L.; Pelta, J. Dynamics of Completely Unfolded and Native Proteins through Solid-State Nanopores as a Function of Electric Driving Force. *ACS Nano* **2011**, *5*, 3628–3638.
- (24) Freedman, K. J.; Jürgens, M.; Prabhu, A.; Ahn, C. W.; Jemth, P.; Edell, J. B.; Kim, M. J. Chemical, Thermal, and Electric Field Induced Unfolding of Single Protein Molecules Studied Using Nanopores. *Anal. Chem.* **2011**, *83*, 5137–5144.
- (25) Martyushenko, N.; Bell, N. A.; Lamboll, R. D.; Keyser, U. F. Nanopore Analysis of Amyloid Fibrils Formed by Lysozyme Aggregation. *Analyst* **2015**, *140*, 4882–4886.
- (26) Li, W.; Bell, N. A.; Hernández-Ainsa, S.; Thacker, V. V.; Thackray, A. M.; Bujdoso, R.; Keyser, U. F. Single Protein Molecule Detection by Glass Nanopores. *ACS Nano* **2013**, *7*, 4129–4134.
- (27) Wloka, C.; Van Meervelt, V.; van Gelder, D.; Danda, N.; Jager, N.; Williams, C. P.; Maglia, G. Label-Free and Real-Time Detection of Protein Ubiquitination with a Biological Nanopore. *ACS Nano* **2017**, *11*, 4387–4394.
- (28) Hu, R.; Rodrigues, J. V.; Waduge, P.; Yamazaki, H.; Cressiot, B.; Chishti, Y.; Makowski, L.; Yu, D.; Shakhnovich, E.; Zhao, Q.; Wanunu, M. Differential Enzyme Flexibility Probed Using Solid-State Nanopores. *ACS Nano* **2018**, *12*, 4494–4502.
- (29) Luan, B.; Zhou, R. Single-File Protein Translocations through Graphene-MoS<sub>2</sub> Heterostructure Nanopores. *J. Phys. Chem. Lett.* **2018**, *9*, 3409–3415.
- (30) Coulter, W. H. *Means for Counting Particles Suspended in a Fluid*. U.S. Patent US2656508A, October 20, 1953.

- (31) Howorka, S.; Siwy, Z. Nanopore Analytics: Sensing of Single Molecules. *Chem. Soc. Rev.* **2009**, *38*, 2360–2384.
- (32) Wei, R.; Gatterdam, V.; Wieneke, R.; Tampé, R.; Rant, U. Stochastic Sensing of Proteins with Receptor-Modified Solid-State Nanopores. *Nat. Nanotechnol.* **2012**, *7*, 257–263.
- (33) Qin, Z.; Zhe, J.; Wang, G.-X. Effects of Particle's off-Axis Position, Shape, Orientation and Entry Position on Resistance Changes of Micro Coulter Counting Devices. *Meas. Sci. Technol.* **2011**, *22*, 045804.
- (34) Golibersuch, D. C. Observation of Aspherical Particle Rotation in Poiseuille Flow *via* the Resistance Pulse Technique. *Biophys. J.* **1973**, *13*, 265–280.
- (35) Soni, G. V.; Singer, A.; Yu, Z.; Sun, Y.; McNally, B.; Meller, A. Synchronous Optical and Electrical Detection of Biomolecules Traversing through Solid-State Nanopores. *Rev. Sci. Instrum.* **2010**, *81*, 014301.
- (36) Gilboa, T.; Meller, A. Optical Sensing and Analyte Manipulation in Solid-State Nanopores. *Analyst* **2015**, *140*, 4733–4747.
- (37) Ivankin, A.; Henley, R. Y.; Larkin, J.; Carson, S.; Toscano, M. L.; Wanunu, M. Label-Free Optical Detection of Biomolecular Translocation through Nanopore Arrays. *ACS Nano* **2014**, *8*, 10774–10781.
- (38) Kasianowicz, J. J.; Robertson, J. W. F.; Chan, E. R.; Reiner, J. E.; Stanford, V. M. Nanoscopic Porous Sensors. *Annu. Rev. Anal. Chem.* **2008**, *1*, 737–766.
- (39) Pitchford, W. H.; Kim, H.-J.; Ivanov, A. P.; Kim, H.-M.; Yu, J.-S.; Leatherbarrow, R. J.; Albrecht, T.; Kim, K.-B.; Edel, J. B. Synchronized Optical and Electronic Detection of Biomolecules Using a Low Noise Nanopore Platform. *ACS Nano* **2015**, *9*, 1740–1748.
- (40) Balan, A.; Chien, C.-C.; Engelke, R.; Drndic, M. Suspended Solid-State Membranes on Glass Chips with Sub 1-PF Capacitance for Biomolecule Sensing Applications. *Sci. Rep.* **2016**, *5*, 17775.
- (41) Derrington, I. M.; Butler, T. Z.; Collins, M. D.; Manrao, E.; Pavlenok, M.; Niederweis, M.; Gundlach, J. H. Nanopore DNA Sequencing with MspA. *Proc. Natl. Acad. Sci. U. S. A.* **2010**, *107*, 16060.
- (42) Manrao, E. A.; Derrington, I. M.; Laszlo, A. H.; Langford, K. W.; Hopper, M. K.; Gillgren, N.; Pavlenok, M.; Niederweis, M.; Gundlach, J. H. Reading DNA at Single-Nucleotide Resolution with a Mutant MspA Nanopore and Phi29 DNA Polymerase. *Nat. Biotechnol.* **2012**, *30*, 349.
- (43) Craig, J. M.; Laszlo, A. H.; Brinkerhoff, H.; Derrington, I. M.; Noakes, M. T.; Nova, I. C.; Tickman, B. I.; Doering, K.; de Leeuw, N. F.; Gundlach, J. H. Revealing Dynamics of Helicase Translocation on Single-Stranded DNA Using High-Resolution Nanopore Tweezers. *Proc. Natl. Acad. Sci. U. S. A.* **2017**, *114*, 11932.
- (44) Traversi, F.; Raillon, C.; Benameur, S. M.; Liu, K.; Khlybov, S.; Tosun, M.; Krasnozhan, D.; Kis, A.; Radenovic, A. Detecting the Translocation of DNA through a Nanopore Using Graphene Nanoribbons. *Nat. Nanotechnol.* **2013**, *8*, 939.
- (45) Branton, D.; Deamer, D. W.; Marziali, A.; Bayley, H.; Benner, S. A.; Butler, T.; Di Ventra, M.; Garaj, S.; Hibbs, A.; Huang, X.; Jovanovich, S. B.; Krstic, P. S.; Lindsay, S.; Ling, X. S.; Mastrangelo, C. H.; Meller, A.; Oliver, J. S.; Pershin, Y. V.; Ramsey, J. M.; Riehn, R.; Soni, G. V.; Tabard-Cossa, V.; Wanunu, M.; Wiggin, M.; Schloss, J. A. The Potential and Challenges of Nanopore Sequencing. *Nat. Biotechnol.* **2008**, *26*, 1146–1153.
- (46) Carson, S.; Wanunu, M. Challenges in DNA Motion Control and Sequence Readout Using Nanopore Devices. *Nanotechnology* **2015**, *26*, 074004.
- (47) Ying, C.; Houghtaling, J.; Eggenberger, O. M.; Guha, A.; Nirmalraj, P.; Awasthi, S.; Tian, J.; Mayer, M. Formation of Single Nanopores with Diameters of 20–50 Nm in Silicon Nitride Membranes Using Laser-Assisted Controlled Breakdown. *ACS Nano* **2018**, *12*, 11458–11470.
- (48) Plesa, C.; Kowalczyk, S. W.; Zinsmeister, R.; Grosberg, A. Y.; Rabin, Y.; Dekker, C. Fast Translocation of Proteins through Solid State Nanopores. *Nano Lett.* **2013**, *13*, 658–663.
- (49) Dekker, C. Solid-State Nanopores. *Nat. Nanotechnol.* **2007**, *2*, 209–215.
- (50) Balme, S.; Coulon, P. E.; Lepoitevin, M.; Charlot, B.; Yandrapalli, N.; Favard, C.; Muriaux, D.; Bechelany, M.; Janot, J.-M. Influence of Adsorption on Proteins and Amyloid Detection by Silicon Nitride Nanopore. *Langmuir* **2016**, *32*, 8916–8925.
- (51) Sexton, L. T.; Mukaibo, H.; Katira, P.; Hess, H.; Sherrill, S. A.; Horne, L. P.; Martin, C. R. An Adsorption-Based Model for Pulse Duration in Resistive-Pulse Protein Sensing. *J. Am. Chem. Soc.* **2010**, *132*, 6755–6763.
- (52) Galenkamp, N. S.; Soskine, M.; Hermans, J.; Wloka, C.; Maglia, G. Direct Electrical Quantification of Glucose and Asparagine from Bodily Fluids Using Nanopores. *Nat. Commun.* **2018**, *9*, 4085.
- (53) Van Meervelt, V.; Soskine, M.; Singh, S.; Schuurman-Wolters, G. K.; Wijma, H. J.; Poolman, B.; Maglia, G. Real-Time Conformational Changes and Controlled Orientation of Native Proteins Inside a Protein Nanoreactor. *J. Am. Chem. Soc.* **2017**, *139*, 18640–18646.
- (54) Waduge, P.; Hu, R.; Bandarkar, P.; Yamazaki, H.; Cressiot, B.; Zhao, Q.; Whitford, P. C.; Wanunu, M. Nanopore-Based Measurements of Protein Size, Fluctuations, and Conformational Changes. *ACS Nano* **2017**, *11*, 5706–5716.
- (55) Lee, J.; Bayley, H. Semisynthetic Protein Nanoreactor for Single-Molecule Chemistry. *Proc. Natl. Acad. Sci. U. S. A.* **2015**, *112*, 13768–13773.
- (56) Sha, J.; Si, W.; Xu, B.; Zhang, S.; Li, K.; Lin, K.; Shi, H.; Chen, Y. Identification of Spherical and Nonspherical Proteins by a Solid-State Nanopore. *Anal. Chem.* **2018**, *90*, 13826–13831.
- (57) Robertson, J. W.; Rodrigues, C. G.; Stanford, V. M.; Rubinson, K. A.; Krasnikov, O. V.; Kasianowicz, J. J. Single-Molecule Mass Spectrometry in Solution Using a Solitary Nanopore. *Proc. Natl. Acad. Sci. U. S. A.* **2007**, *104*, 8207–8211.
- (58) Sexton, L. T.; Horne, L. P.; Sherrill, S. A.; Bishop, G. W.; Baker, L. A.; Martin, C. R. Resistive-Pulse Studies of Proteins and Protein/Antibody Complexes Using a Conical Nanotube Sensor. *J. Am. Chem. Soc.* **2007**, *129*, 13144–13152.
- (59) Han, A.; Creus, M.; Schürmann, G.; Linder, V.; Ward, T. R.; de Rooij, N. F.; Staufer, U. Label-Free Detection of Single Protein Molecules and Protein-Protein Interactions Using Synthetic Nanopores. *Anal. Chem.* **2008**, *80*, 4651–4658.
- (60) Fologea, D.; Ledden, B.; McNabb, D. S.; Li, J. Electrical Characterization of Protein Molecules by a Solid-State Nanopore. *Appl. Phys. Lett.* **2007**, *91*, 053901.
- (61) Giambanco, N.; Coglitore, D.; Janot, J.-M.; Coulon, P. E.; Charlot, B.; Balme, S. Detection of Protein Aggregate Morphology through Single Antifouling Nanopore. *Sens. Actuators, B* **2018**, *260*, 736–745.
- (62) Lepoitevin, M.; Ma, T.; Bechelany, M.; Balme, S.; Janot, J.-M. Functionalization of Single Solid State Nanopores to Mimic Biological Ion Channels: A Review. *Adv. Colloid Interface Sci.* **2017**, *250*, 195–213.
- (63) Talaga, D. S.; Li, J. Single-Molecule Protein Unfolding in Solid State Nanopores. *J. Am. Chem. Soc.* **2009**, *131*, 9287–9297.
- (64) Luan, B.; Wang, D.; Zhou, R.; Harrer, S.; Peng, H.; Stolovitzky, G. Dynamics of DNA Translocation in a Solid-State Nanopore Immersed in Aqueous Glycerol. *Nanotechnology* **2012**, *23*, 455102.
- (65) Yusko, E. C.; Johnson, J. M.; Majd, S.; Prangko, P.; Rollings, R. C.; Li, J.; Yang, J.; Mayer, M. Controlling Protein Translocation through Nanopores with Bio-Inspired Fluid Walls. *Nat. Nanotechnol.* **2011**, *6*, 253–260.
- (66) Rosenstein, J. K.; Wanunu, M.; Merchant, C. A.; Drndic, M.; Shepard, K. L. Integrated Nanopore Sensing Platform with Sub-Microsecond Temporal Resolution. *Nat. Methods* **2012**, *9*, 487.
- (67) Fricke, H. The Electric Permittivity of a Dilute Suspension of Membrane-Covered Ellipsoids. *J. Appl. Phys.* **1953**, *24*, 644–646.

- (68) Velick, S.; Gorin, M. The Electrical Conductance of Suspensions of Ellipsoids and Its Relation to the Study of Avian Erythrocytes. *J. Gen. Physiol.* **1940**, *23*, 753.
- (69) Di Fiori, N.; Squires, A.; Bar, D.; Gilboa, T.; Moustakas, T. D.; Meller, A. Optoelectronic Control of Surface Charge and Translocation Dynamics in Solid-State Nanopores. *Nat. Nanotechnol.* **2013**, *8*, 946.
- (70) Nir, I.; Huttner, D.; Meller, A. Direct Sensing and Discrimination among Ubiquitin and Ubiquitin Chains Using Solid-State Nanopores. *Biophys. J.* **2015**, *108*, 2340–2349.
- (71) DeBlois, R. W.; Uzgiris, E. E.; Cluxton, D. H.; Mazzone, H. M. Comparative Measurements of Size and Polydispersity of Several Insect Viruses. *Anal. Biochem.* **1978**, *90*, 273–288.
- (72) Smythe, W. R. Flow around a Spheroid in a Circular Tube. *Phys. Fluids* **1964**, *7*, 633–638.
- (73) Yusko, E. C.; Billeh, Y. N.; Yang, J.; Mayer, M. Nanopore Recordings to Quantify Activity-Related Properties of Proteins. In *Nanopores: Sensing and Fundamental Biological Interactions*; Iqbal, S. M., Bashir, R., Eds.; Springer US: Boston, MA, 2011; pp 203–225.
- (74) *Single Molecules and Nanotechnology*; Rigler, R., Vogel, H., Eds.; Springer Series in Biophysics; Springer Berlin Heidelberg: Berlin, Germany, 2008; Vol. 12.
- (75) Uram, J. D.; Ke, K.; Mayer, M. Noise and Bandwidth of Current Recordings from Submicrometer Pores and Nanopores. *ACS Nano* **2008**, *2*, 857–872.
- (76) García de la Torre, J.; Huertas, M. L.; Carrasco, B. Calculation of Hydrodynamic Properties of Globular Proteins from Their Atomic-Level Structure. *Biophys. J.* **2000**, *78*, 719–730.
- (77) Dix, J. A.; Verkman, A. S. Crowding Effects on Diffusion in Solutions and Cells. *Annu. Rev. Biophys.* **2008**, *37*, 247–263.
- (78) Li, J.; Stein, D.; McMullan, C.; Branton, D.; Aziz, M. J.; Golovchenko, J. A. Ion-Beam Sculpting at Nanometre Length Scales. *Nature* **2001**, *412*, 166–169.
- (79) Oncley, J. L. The Investigation of Proteins by Dielectric Measurements. *Chem. Rev.* **1942**, *30*, 433–450.
- (80) Yuan, Y.; Axelrod, D. Subnanosecond Polarized Fluorescence Photobleaching: Rotational Diffusion of Acetylcholine Receptors on Developing Muscle Cells. *Biophys. J.* **1995**, *69*, 690–700.
- (81) Singh, S. N.; Yadav, S.; Shire, S. J.; Kalonia, D. S. Dipole-Dipole Interaction in Antibody Solutions: Correlation with Viscosity Behavior at High Concentration. *Pharm. Res.* **2014**, *31*, 2549–2558.
- (82) Ling, D. Y.; Ling, X. S. On the Distribution of DNA Translocation Times in Solid-State Nanopores: An Analysis Using Schrödinger's First-Passage-Time Theory. *J. Phys.: Condens. Matter* **2013**, *25*, 375102.
- (83) Li, X.; Hu, R.; Li, J.; Tong, X.; Diao, J. J.; Yu, D.; Zhao, Q. Non-Sticky Translocation of Bio-Molecules through Tween 20-Coated Solid-State Nanopores in a Wide PH Range. *Appl. Phys. Lett.* **2016**, *109*, 143105.
- (84) Firnkens, M.; Pedone, D.; Knezevic, J.; Döblinger, M.; Rant, U. Electrically Facilitated Translocations of Proteins through Silicon Nitride Nanopores: Conjoint and Competitive Action of Diffusion, Electrophoresis, and Electroosmosis. *Nano Lett.* **2010**, *10*, 2162–2167.
- (85) Galla, L.; Meyer, A. J.; Spiering, A.; Sischka, A.; Mayer, M.; Hall, A. R.; Reimann, P.; Anselmetti, D. Hydrodynamic Slip on DNA Observed by Optical Tweezers-Controlled Translocation Experiments with Solid-State and Lipid-Coated Nanopores. *Nano Lett.* **2014**, *14*, 4176–4182.
- (86) Sischka, A.; Galla, L.; Meyer, A. J.; Spiering, A.; Knust, S.; Mayer, M.; Hall, A. R.; Beyer, A.; Reimann, P.; Götzhäuser, A.; Anselmetti, D. Controlled Translocation of DNA through Nanopores in Carbon Nano-, Silicon-Nitride- and Lipid-Coated Membranes. *Analyst* **2015**, *140*, 4843–4847.
- (87) Berge, L. I.; Jossang, T.; Feder, J. Off-Axis Response for Particles Passing through Long Apertures in Coulter-Type Counters. *Meas. Sci. Technol.* **1990**, *1*, 471.
- (88) Smythe, W. R. Off-Axis Particles in Coulter Type Counters. *Rev. Sci. Instrum.* **1972**, *43*, 817–818.
- (89) Guo, J.; Pui, T. S.; Rahman, A. R. A.; Kang, Y. 3D Numerical Simulation of a Coulter Counter Array with Analysis of Electrokinetic Forces. *Electrophoresis* **2013**, *34*, 417–424.
- (90) Hinkle, P.; Westerhof, T. M.; Qiu, Y.; Mallin, D. J.; Wallace, M. L.; Nelson, E. L.; Taborek, P.; Siwy, Z. S. A Hybrid Resistive Pulse-Optical Detection Platform for Microfluidic Experiments. *Sci. Rep.* **2017**, *7*, 10173.
- (91) Kozak, D.; Anderson, W.; Grevett, M.; Trau, M. Modeling Elastic Pore Sensors for Quantitative Single Particle Sizing. *J. Phys. Chem. C* **2012**, *116*, 8554–8561.
- (92) Zhang, M. *Numerical Investigation of Hydrodynamic Focusing and Coulter Principle in a Microfluidic Device*. Ph.D. Dissertation, University of Louisville, Louisville, KY, 2014.
- (93) Ecker, D. M.; Jones, S. D.; Levine, H. L. The Therapeutic Monoclonal Antibody Market. *mAbs* **2015**, *7*, 9–14.
- (94) Fraccari, R. L.; Ciccarella, P.; Bahrami, A.; Carminati, M.; Ferrari, G.; Albrecht, T. High-Speed Detection of DNA Translocation in Nanopipettes. *Nanoscale* **2016**, *8*, 7604–7611.
- (95) Tabard-Cossa, V.; Trivedi, D.; Wiggin, M.; Jetha, N. N.; Marziali, A. Noise Analysis and Reduction in Solid-State Nanopores. *Nanotechnology* **2007**, *18*, 305505.
- (96) Roelen, Z.; Bustamante, J. A.; Carlsen, A.; Baker-Murray, A.; Tabard-Cossa, V. Instrumentation for Low Noise Nanopore-Based Ionic Current Recording under Laser Illumination. *Rev. Sci. Instrum.* **2018**, *89*, 015007.
- (97) De Vreede, L.; Ying, C.; Houghtaling, J.; Figueiredo Da Silva, J.; Hall, A. R.; Lovera, A.; Mayer, M. Wafer Scale Fabrication of Fused Silica Chips for Low-Noise Recording of Resistive Pulses through Nanopores. *Nanotechnology* **2019**, *30*, 265301.
- (98) Wanunu, M.; Meller, A. Chemically Modified Solid-State Nanopores. *Nano Lett.* **2007**, *7*, 1580–1585.
- (99) Tang, Z.; Lu, B.; Zhao, Q.; Wang, J.; Luo, K.; Yu, D. Surface Modification of Solid-State Nanopores for Sticky-Free Translocation of Single-Stranded DNA. *Small* **2014**, *10*, 4332–4339.
- (100) Giambianco, N.; Coglitore, D.; Gubbiotti, A.; Ma, T.; Balanzat, E.; Janot, J.-M.; Chinappi, M.; Balme, S. Amyloid Growth, Inhibition, and Real-Time Enzymatic Degradation Revealed with Single Conical Nanopore. *Anal. Chem.* **2018**, *90*, 12900–12908.
- (101) Thakur, A. K.; Movileanu, L. Real-Time Measurement of Protein-Protein Interactions at Single-Molecule Resolution Using a Biological Nanopore. *Nat. Biotechnol.* **2018**, *37*, 96–101.
- (102) Prangio, P.; Yusko, E. C.; Sept, D.; Yang, J.; Mayer, M. Multivariate Analyses of Amyloid-Beta Oligomer Populations Indicate a Connection between Pore Formation and Cytotoxicity. *PLoS One* **2012**, *7*, No. e47261.
- (103) De Pascalis, A. R.; Jelesarov, I.; Ackermann, F.; Bosshard, H. R.; Koppenol, W. H.; Hirasawa, M.; Knaff, D. B. Binding of Ferredoxin to Ferredoxin: NADP+ Oxidoreductase: The Role of Carboxyl Groups, Electrostatic Surface Potential, and Molecular Dipole Moment. *Protein Sci.* **1993**, *2*, 1126–1135.
- (104) Yang, J.; Ferranti, D. C.; Stern, L. A.; Sanford, C. A.; Huang, J.; Ren, Z.; Qin, L.-C.; Hall, A. R. Rapid and Precise Scanning Helium Ion Microscope Milling of Solid-State Nanopores for Biomolecule Detection. *Nanotechnology* **2011**, *22*, 285310.
- (105) Pedone, D.; Firnkens, M.; Rant, U. Data Analysis of Translocation Events in Nanopore Experiments. *Anal. Chem.* **2009**, *81*, 9689–9694.